

# Flow separations in blood flow—its significance in the human circulation system and in artificial organs

U. Kertzscher, L. Goubergrits & K. Affeld

*Biofluidmechanics Laboratory, Charité, University Medicine Berlin, Germany.*

## Abstract

Flow separations are ubiquitous in daily life and engineering. In most cases, they are unwelcome and impede the performance of the devices in which they occur. The flow separates inevitably behind bluff bodies. This increases the drag. In aircraft flow separation at the wings may even lead to a loss of stability and a catastrophic crash. In pumps and turbines vibrations may occur, while in tubing systems a loss of energy is observed. How does nature handle this flow phenomenon? Specifically, how is the circulatory system of the human body adapted? In the human body, the blood leaves the heart and enters the circulatory loop with a velocity of about 1 m/s. At the other end, in the capillaries, the blood moves at a speed of only 1 mm/s. This is achieved by the increase of the total cross-section area of the vessels. This enormous deceleration occurs in the major part of the blood circulation without flow separations. The reason is that area enlargement occurs normally at bifurcations. However, at some vessels and bifurcations, some flow separations with large areas of low wall shear stress still do occur. The combination of low wall shear stress—as it occurs in flow separation—and certain blood components cause the wall of the blood vessel to change its nature. These changes make the inner surface rough and decrease the cross section, a process called arteriosclerosis. A host of impairments result from these changes of the vessel wall. This affects a large number of people in modern western society. The eminent German pathologist R. Virchow discovered the interaction of flow, blood contents and the vessel wall more than 150 years ago. To date, the ‘Virchow’s Triad’ is not completely understood. Using modern tools in experimental and numerical fluid mechanics great progress has been made in the elucidation of pathological events. At the core of it, a low wall shear stress, mostly caused by a flow separation, is always found.

## 1 Introduction—nature of flow separation

Flow separations are ubiquitous in daily life and engineering. Furthermore, this flow phenomenon is very crucial for many pathologic processes in blood circulation. However, before we consider



the problem of flow separation in blood flow, we have to understand the nature of this flow phenomenon. In most cases, flow separations are unwelcome and impede the performance of the devices in which they occur. The problem of flow separation is mainly concerned with design and optimization of vehicles.

The philosophy of good aircraft, good cars or good pipelines is primarily derived from the philosophy that good aero- or hydrodynamics has low drag [1]. It is not difficult to design an airplane with sufficient lift for flight; the challenge is to obtain this lift with as little drag as possible. The aerodynamic parameters of a body are described by force and moment coefficients. The lift, drag, and moment coefficients for a given body, denoted by  $C_L$ ,  $C_D$ , and  $C_M$ , respectively, are defined as follows:

$$C_L = \frac{L}{q_\infty S}; \quad C_D = \frac{D}{q_\infty S}; \quad C_M = \frac{M}{cq_\infty S}, \quad (1)$$

where  $L$ ,  $D$ , and  $M$  denote the lift, drag, and moment of a body.  $S$  is the size of the body, which is denoted by a reference area,  $c$  is a characteristic length of the body, and  $q_\infty$  is the dynamic pressure, which is defined using the density  $\rho$  of an ambient fluid and the velocity of the body  $V_\infty$  as:

$$q_\infty = \rho \frac{V_\infty^2}{2}. \quad (2)$$

Using the powerful method of dimensional analysis we obtain the following results for the dependence of the coefficients on parameters:

$$\begin{aligned} C_L &= f_L(\alpha, \text{Re}, M_\infty), \\ C_D &= f_D(\alpha, \text{Re}, M_\infty), \\ C_M &= f_M(\alpha, \text{Re}, M_\infty), \end{aligned} \quad (3)$$

where  $\alpha$  is the angle of attack (orientation of the body relative to the direction of motion of the body). Reynolds number  $\text{Re}$  and Mach number  $M_\infty$  are similarity parameters defined as:

$$\text{Re} = \frac{\rho_\infty V_\infty c}{\mu_\infty}, \quad (4)$$

$$M_\infty = \frac{V_\infty}{a_\infty}, \quad (5)$$

where  $\mu_\infty$  is the viscosity coefficient and  $a_\infty$  is the speed of sound in the fluid which is a measure of the compressibility. We could run a series of wind tunnel tests in which we obtain the lift and drag coefficients as a function of  $\alpha$ , keeping  $\text{Re}$  and  $M_\infty$  constant. The results show that the lift coefficient increases essentially linearly with angle of attack over most of the practical range. However, since the end of 19th century it has been known that an increase of the lift force by airfoils is limited. From some angle of attack the lift force falls drastically, whereas the drag force increases significantly. The cause of this phenomenon is a flow separation on the airfoil [2] as shown in Fig. 1.

In aircraft a flow separation at the wings may even lead to stability loss and a catastrophic crash. Flow separations are also found in ships, cars, trains and buildings. The flow separates inevitably behind bluff bodies. This increases the drag which results in higher fuel consumption. In pumps and turbines vibrations caused by flow separations may occur, whereas in pipelines for gas or oil transport a loss of energy is observed. All these problems are encountered in engineering.



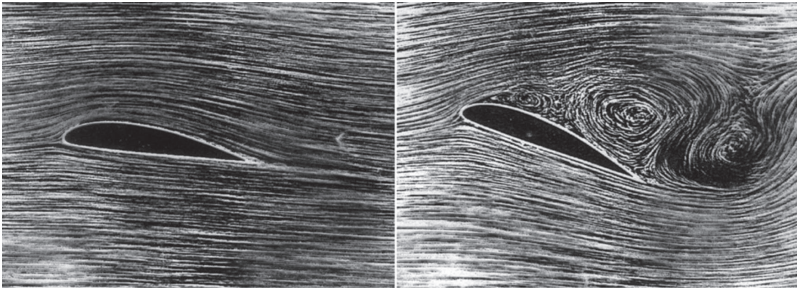


Figure 1: Visualization of the flow over an airfoil under low angle of attack (left) and under high angle of attack (right) [2].

What about flow separations in living organisms? Do they occur in the human blood flow? And if so, how does the circulatory system deal with this flow phenomenon?

In general, there is no difference in the flow separation phenomenon occurring in the pipelines and in the circulatory system with regard to fluid mechanics. The main objective of both the technical and the biological system is transport. Both are channel flows, whose geometries incorporate bifurcations, bends and obstacles (valves), all of which may cause flow separations. However, there is one important difference between this flow phenomenon in engineering and in living organisms. In engineering the formation of flow separation usually impedes only the function of the device and rarely causes a destruction of the device. In living organisms, however, flow separation may result in pathological events threatening the life of a person. This is caused by the strong interaction between flow, fluid (blood) and geometry (vessel walls) resulting in thrombus formation, arteriosclerosis, vessel enlargement (vasodilatation) and intimal hyperplasia in coronary artery bypass grafts. The eminent German pathologist R. Virchow was first to observe and formulate the interaction of flow, blood contents and the vessel wall about 150 years ago [3]. The so-called ‘Virchow’s Triad’ has been confirmed by clinical observations ever since. However, this interaction is not fully understood in its depth, but some progress has been made using modern tools of experimental and numerical fluid mechanics. The main result is that flow separation is the culprit behind these pathological events. At the core of it, a low wall shear stress, mostly caused by a flow separation, is always found. All these effects will be discussed in more detail in Section 2. Now we concentrate on the question: What is flow separation and how does it occur?

Figure 1 illustrates the phenomenon of flow separation. Both images show a two-dimensional flow past an airfoil. The image on the left shows the flow past an airfoil which is under a low angle of attack. The fluid follows the airfoil till the rear where the upper side flow and the lower side flow join again. The boundary layers from both sides meet and form a vortex sheet downstream of the body. For this configuration the drag will be very low. Such bodies are said to be streamlined. The drag on a streamlined body can be lower by a factor of 15 than on a cylinder of the same thickness [1]. The most important features are the slowly tapering tail and the low angle of attack. The image on the right shows the flow past the same airfoil, under a high angle of attack. Separation occurs on the upper side of the airfoil forming a large separation bulge, which is a region of fluctuating recirculations. These fluctuations may cause airfoil oscillations and noise emissions. How is this flow separation generated? Fluid initially close to the wall and moving in the main flow direction (from left to right) suddenly detaches from the wall; further along the boundary the flow is in the opposite direction, as part of a recirculation region. The streamline pattern is shown in Fig. 2. The flow is said to separate, and the point S is called the separation point.

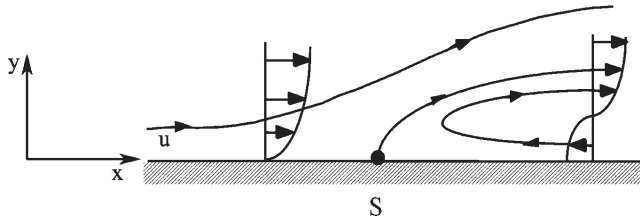


Figure 2: Typical streamline pattern in the vicinity of the separation point S. The main flow direction is from left to right.

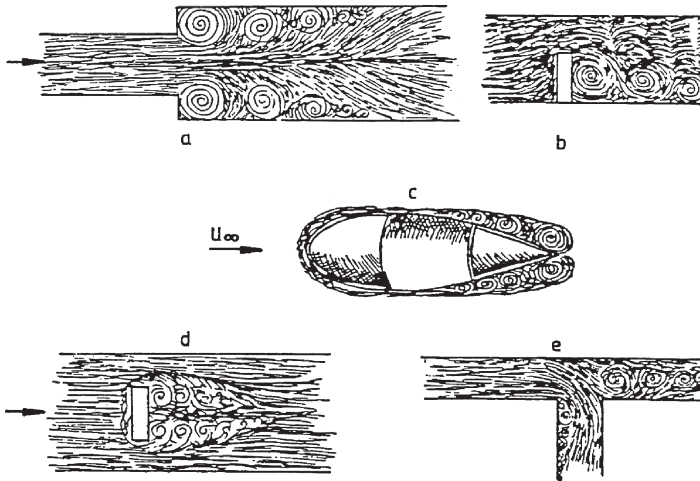


Figure 3: Five different types of flow separation phenomena sketched by Leonardo da Vinci. (a) Flow separations in the sudden duct enlargement; (b), (c) and (d) flow separation behind obstacles in the flow; (e) flow separation in a bifurcation [2].

The distinction between points on the wall to the left and right of point S is in the sign of shear rate  $\gamma$ , which is defined as:

$$\gamma = \left( \frac{\partial u}{\partial y} \right)_{y=0} \tag{6}$$

S is thus defined as the point at which the shear rate is zero.

The interest of scientists in this phenomenon dates back to the 16th century. In the early 16th century Leonardo da Vinci investigated some problems of hydrodynamics regarding irrigation. Some of his observations were sketched in drawings.

Figure 3 shows five examples of channel flows and flows past bodies, showing the vortex formations in the flow separation region. Some of Leonardo da Vinci’s insights concerning these images are considered in the paper by Flachsbart [4]. Leonardo da Vinci described his observations of the flow formations behind obstacles in the river, which were also sketched, thus: ‘So moving water strives to maintain the course pursuant to the power which occasions it and, if it finds an obstacle in its path, completes the span of the course it has commenced by a circular and revolving movement.’ Some researchers consider these words to be the first description of turbulence. The advantages of investigations on flow separation phenomena in the 20th century and now are

mainly related with the development of new methods of velocity measurements with high time and space resolution such as laser Doppler velocimetry or hot-wire anemometry. To date there is no exact mathematical theory for the description of flow separation, which is phenomenologically subdivided into different types. Typically, in fluid dynamics it is classified by flow (laminar, transient or turbulent) and by geometry, both defining the boundary conditions. A more detailed description of flow separation classification can be found in [2].

Flow separation is a phenomenon that can occur under low and high Reynolds numbers. For several reasons separation at high Reynolds number, i.e. boundary layer separation, received more attention than low Reynolds number separation. The reason for this is that high Reynolds number flows are encountered more widely. Airplane, car and ship flows are high Reynolds number flows. Furthermore, the boundary layer separation has more profound consequences for the whole flow structure as a separation on the bluff bodies. As a result, explanations for flow separation are mainly described as a boundary layer separation. However, the fact remains that separation does not always suggest boundary layer separation and so it deserves a more general approach.

In order to discuss conditions for separation, let us consider steady two-dimensional flow. For this case, we can rewrite the Navier–Stokes equation for vorticity [eqn (7)] by applying the curl operation:

$$u \cdot \nabla \zeta = \frac{\mu}{\rho} \nabla^2 \zeta, \quad (7)$$

where  $\zeta$  is vorticity component in  $z$ -direction defined by:

$$\zeta = \frac{\partial v}{\partial x} - \frac{\partial u}{\partial y}. \quad (8)$$

At the wall,  $y=0$ , one has  $u=0$  and  $v=0$  for all  $x$ , resulting in the fact that at the wall the first component of eqn (8) is zero. This means from eqn (6) that the vorticity changes sign at the separation point  $S$ . Consider now the Navier–Stokes equation at the boundary ( $y=0$ ):

$$\frac{1}{\rho} \frac{\partial p}{\partial x} = \frac{\mu}{\rho} \frac{\partial \zeta}{\partial y}. \quad (9)$$

Equation (9) tells us that there is a region with positive pressure gradient related to the separation region. This is a necessary but not a sufficient condition for separation. A further important point is that, without vorticity diffusion, there is no mechanism for a region with positive vorticity, as seen from eqn (7). Hence, the existence of viscous effects in the flow is needed for a flow separation. The question of whether the separation will occur is, first, a question of whether the flow develops the region of positive pressure gradient and, second, whether this is large enough. The answer to the second question is almost always difficult. It was Prandtl who, based on his boundary layer approximation, found these conditions for flow separations [5].

For consideration of flow separation in the blood circulation system, an alternative explanation for the positive pressure gradient in diverging channels is required. The separation may also occur on the rear part of the obstacle placed in the flow and on the walls of the diverging channel, which may be explained by Bernoulli's equation governing inviscid flows. Following Bernoulli's equation, any divergence that causes velocity reduction, as it follows from the mass conservation law, results in a positive pressure gradient, which may cause flow separation.



## 2 Flow separation in the human circulation system

### 2.1 Blood flow and separation in the circulation system of mammals

The main function of the blood circulation system is transporting blood throughout the body. The blood circulation system, which is a convection system, carries out its function by means of a network characterized by vessel branching, valves defining flow direction, curved vessel segments and moving walls as found in the heart, which is a muscular pump.

The heart is the central organ of blood circulation and its trouble-free function is crucial for the whole body function, because it supplies the power to pump blood throughout the circulation system which provides the body with oxygen and nutrients. The mammalian heart consists of two pumps, connected to each other in series. During embryonic development it first forms a single structure and later the pumps remain connected anatomically. These two pumps form the left and the right hearts, which are divided by a septum. Each of these hearts consists of a low-pressure chamber (atrium), which is filled by a vein and is connected to a high-pressure chamber (ventricle) via valves. The ventricle pumps blood through a second valve into an arterial system. The valves separating the atriums from the ventricles differ slightly anatomically but are similar in function and structure. The atrioventricular valve of the right heart (the tricuspidal valve) has three cusps, while that of the left heart (the mitral valve) has two. The extremely thin cusps (about 0.1 mm) consist of flaps, attached along one edge to a fibrous ring and free edges directed into the ventricles and tethered to the wall by fibrous bands. The cusps are made of a meshwork of collagen and elastin fibers, covered by a layer of cells similar to the cells lining the walls of the heart and the vessels—the endothelial cells. The exit valves from the ventricles (pulmonary and aortic valves) are similar to each other, each consisting of three cusps. The cusps are not tethered but attached directly to the arterial wall. In the case of the aortic valve this pressure difference is about 100 mmHg. The valves are very efficient, having a small resistance and only minor backflow occurs during closure. All heart valves open and close more than 30 million times in a year.

The heart pumps the blood against a systemic pressure, which is about 100 mmHg (13 kPa). The power needed for this work is the product of the pressure drop in the system, which is nearly equal to the mean systemic pressure, and the volume flow of the blood, which varies between 5 l/min at rest and 25 l/min during exercise. The required flow volume is defined by the metabolic rate  $\Gamma$  (W), which is a function of body mass and is approximated as follows:

$$\Gamma = b3.6M^{3/4}, \quad (10)$$

where  $M$  is the body mass and  $b$  is a dimensional constant depending on the activity and varying between 1 (for rest) and 15. Typically, for a man, the heart power at rest is  $P = 1.1$  W, i.e. a small fraction of the total metabolic rate at rest (87 W for a man with body mass of 70 kg [6]).

From a hemodynamic point of view, there are two main tasks related to heart function: increase of the systemic pressure that is related with vascular system problems and a loss of valve functions. Both tasks may be only partially performed by increased heart power. The problems of the vascular system are discussed in Section 2.2.2, whereas valve-related problems are discussed in Section 2.2.1.

As we mentioned above, the blood circulation system is a network system of branching vessels that act as pipelines for convective blood transport through the body. However, the final transport of oxygen and nutrients to tissues is done by diffusion, which is restricted by distance. Oxygen molecules need 0.0054 s to cover a distance of 7  $\mu\text{m}$ , 54 s to cover 0.7 mm and more than 11,000 s to cover a distance of 10 mm. Hence, a huge network of fine capillaries with thin walls is needed



Table 1: Some parameters of the vessel system of a dog of 13 kg weight [8].

Vessel	Diameter (mm)	Number	Total cross section (cm <sup>2</sup> )	Length (cm)	Total volume (ml)
Aorta	10	1	0.8	40	30
Large artery	3	40	3.0	20	60
Middle artery	1	600	5.0	10	50
Small artery	0.6	1800	5.0	1.0	5
Arteriole	0.02	40000000	125	0.2	25
Capillary	0.008	1200000000	600	0.1	60
Venule	0.03	80000000	570	0.2	110
Small vein	1.5	1800	30	1.0	30
Vein	2.4	600	27	10	270
Large vein	6	40	11	20	220
Vein cava	12.5	1	1.2	40	50

for the transport of oxygen and nutrients from vessels to tissues. Table 1 gives an overview of the vessel system in a dog. Table 1 shows that the circulation system, which starts from the left ventricle with the aorta, steadily increases the total cross-section area. This is due to the drastic increase in the number of parallel branches by a decrease of the vessel diameter all the way down to the smallest vessels—capillaries. This cross-sectional increase by a large number of vessels requires a huge number of bifurcations. After each bifurcation, the combined cross-section area of the branches is normally larger than the cross-section area of the parent vessel. The total length of all vessel segments in the circulation system of the dog is more than 1,400 km.

The pressure drop in a vessel is caused by viscous fluid forces and depends on the nature of the flow. Flow through a pipe can be slow and uniform, called laminar, or fast and chaotic called turbulent. In both cases the fluid adheres to the wall and its velocity is zero at the wall surface. This velocity increases with the distance from the wall. The farther away from the wall the faster the fluid can move. In the case of laminar flow the velocity profile forms a parabola. The pressure difference that is needed to overcome these viscous forces depends on the flow. The flow is characterized by the dimensionless Reynolds number (4), which is the ratio of inertial forces and viscous forces. Flow in a pipe becomes turbulent if the Reynolds number exceeds the critical value  $Re_{cr} \approx 2300$  [1]. The range of Reynolds numbers in the blood circulation system varies significantly from 10,000 during peak systole in the aorta to 0.002 in the capillaries [7]. In the human circulation system, the largest Reynolds number is found in the aortic root and is normally about  $Re = 6000$  which indicates turbulence. However, in most of the remaining part of the circulatory system the flow is laminar, especially in the capillary system, where 80% of the total systemic pressure drop takes place [8].

The pressure drop  $dp$  in a duct with laminar flow is expressed by the Hagen Poiseuille equation:

$$\Delta p = \frac{\dot{V} \cdot L \cdot 8 \cdot \mu}{\pi \cdot a^4 \cdot \rho}, \quad (11)$$

where  $\dot{V}$  is the volume flow rate,  $L$  is the segment length and  $a$  is the segment radius. According to this equation, a pipeline of 1,400 km length will cause a huge pressure drop if all the capillaries are connected in series. However, they form a network with the capillaries connected in parallel.



For this Kirchhoff’s law is applied, which defines the total resistance  $R_t$  of  $N$  parallel connected segments:

$$\frac{1}{R_t} = \frac{1}{R_1} + \frac{1}{R_2} + \dots + \frac{1}{R_N}. \tag{12}$$

From this equation we find that 100 equivalent segments connected in parallel cause a pressure drop that is reduced by factor 100 compared with the pressure drop of one segment. Note that such a network can only be realized with an appropriate, large, number of bifurcations.

Equations (11) and (12) mainly define the systemic pressure drop and hence the power which the heart needs to generate the required blood flow rate, which is called the cardiac output. However, in pipelines there are also some additional geometric formations which may cause an increase of pressure drop. These formations are vessel enlargements and bends. Both are well known and well investigated in engineering, because these formations are unavoidable in a complex system of pipelines.

In duct enlargement, as we noted in Section 1, the increase in cross section results in a decrease of velocity and as per Bernoulli’s equation leads to an increase of static pressure. The generated positive pressure gradient increases the danger of flow separation. The separated flow forms a recirculation region. The loss of energy needed for recirculation is higher with a larger cross-section enlargement. For duct enlargement, as shown in Fig. 4 (left), the energy loss or pressure drop caused by flow separation is expressed by the following equation:

$$\Delta p = \zeta \cdot \rho \cdot \frac{V^2}{2}, \tag{13}$$

where  $V$  is the mean inlet velocity and  $\zeta$  is the so-called loss parameter, which characterizes the effect of duct enlargement. For sudden duct enlargement (enlargement with angle  $\alpha = 180^\circ$ ), the parameter  $\zeta$  is described by the Borda–Carnot equation [9]:

$$\zeta = (En - 1)^2, \tag{14}$$

where the enlargement parameter  $En$  is the ratio of the outlet to the inlet cross-section area— $En = A_{out}/A_{in}$ . In the case of continuous enlargement, there is an additional coefficient  $\eta$ , which

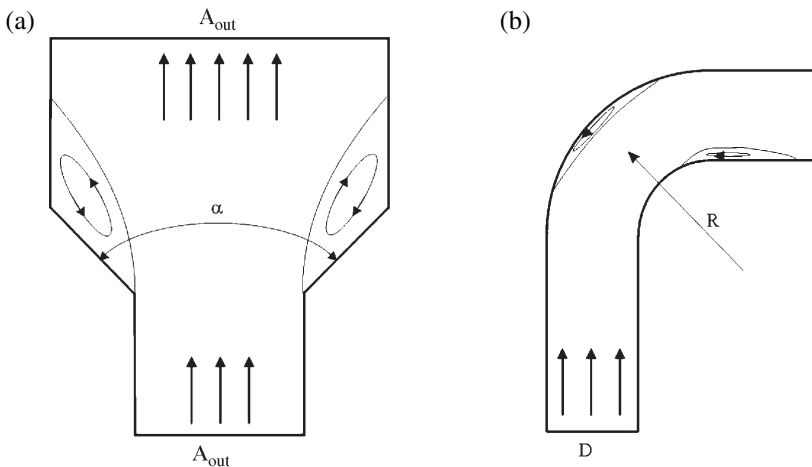


Figure 4: (a) Drawing of a duct enlargement. (b) Drawing of a 90° duct bend with curvature radius  $R$  and duct diameter  $D$ . Arrows show the flow direction.





depends on the enlargement angle  $\alpha$ . The loss parameter  $\zeta$  is then described by the following equation:

$$\zeta = \eta(\alpha) \cdot (\text{En} - 1)^2. \quad (15)$$

For duct enlargement, the parameter  $\eta$  is about 0.15–0.2 for enlargement angles  $\alpha = 8^\circ$ – $10^\circ$ . However, for relatively small angles,  $\alpha = 24^\circ$ , the parameter  $\eta$  increases up to  $\approx 0.64$  and from eqn (14) it follows that  $\eta = 1$  for sudden expansion [9]. Note that the loss parameter for duct enlargement may be higher than 1.

In duct bends, as shown in Fig. 4 (right), geometry curved streamlines cause centrifugal forces to act on the fluid. These forces generate pressure differences across the cross section of the curved duct. Two regions of flow separation, one at the outer and the other at the inner side of the duct, are formed as shown in Fig. 4 (right). At the same time secondary flow in the form of two counter-rotating vortices is formed.

Note that in the blood circulation system the continuous increase in the total cross-section area from aorta to capillaries take place in bifurcations. Hence, two geometric formations, which cause additional pressure drops in the vascular system, are bifurcations and bends. The energy loss or pressure drop caused by flow separations in bends is also expressed by eqn (13). The loss parameter  $\zeta$  is a function of two geometric parameters: the angle of bending  $\delta$  and the ratio of the curvature radius  $R$  and the duct diameter  $D$ , which can be expressed by the following equation [9]:

$$\zeta = K(\delta) \cdot \zeta_{90}(R/D), \quad (16)$$

where  $\zeta_{90}$  is the loss parameter for a  $90^\circ$  bend. The parameter  $K$  varies between 0.44 for  $\delta = 30^\circ$  and 1.68 for  $\delta = 180^\circ$ . The experiments by A. Hoffmann with a  $90^\circ$  bend of circular cross-section show that the loss parameter  $\zeta_{90}$  varies slightly for  $R/D > 4$  and is  $\approx 0.1$ . For comparison, a similar loss parameter is achieved in sudden duct enlargement with enlargement  $\text{En} = 1.31$ . For bends with smaller curvature radius or  $R/D < 4$ , the loss parameter increases up to 0.5 with decreased parameter  $R/D$ . The maximum possible value for the pressure loss parameter is about  $\zeta = 1$  for a  $180^\circ$  bend with normalized curvature radius  $R/D = 1$ . The  $180^\circ$  bend occurs, for example, in the aorta (see Fig. 12). For comparison, the loss parameter  $\zeta = 1$  may be achieved in a sudden duct enlargement with  $\text{En} = 2$ . However, in the blood circulation system there are enlargements with  $\text{En} > 2$ , as shown in Section 2.2.2.

In conclusion, there are two main geometric parameters, which may cause an increase of pressure drop in a duct flow and hence in blood circulating systems due to flow separation. These parameters are the duct enlargement  $\text{En} = A_{\text{out}}/A_{\text{in}}$  and the normalized duct curvature radius  $R/D$ . However, a significant increase in pressure drop takes place only for enlargements  $\text{En} > 1.3$  and normalized curvature radii  $R/D < 4$ .

## 2.2 Problems in the human circulation system caused by separation

### 2.2.1 Flow separation and thrombus formation in a heart valve prosthesis

Trouble-free functioning of heart valves is an important condition for normal heart function and hence normal blood circulation. There are numerous causes for heart valve defects, including inherited defects, bacterial infections, reaction to drugs, and age-associated aortic valve stenosis (narrowing). Rheumatic heart disease can also cause valvular heart problems. Valve thrombosis occurring after heart valve disease, during cardiac catheterization or bacterial endocarditis, may also alter the valve function. Heart valve diseases fall into one of two categories: stenosis, or narrowing of the valve, and insufficiency, or allowing backflow. Stenotic valves cannot open fully



and require more work to push the liquid through the valve. In contrast, incompetent valves waste heart work by allowing blood to flow backward. As a result of stenosis or incompetence, the heart must work harder to provide the same level of blood circulation for the required level of metabolic rate. In many cases the heart becomes incapable of sustaining an active lifestyle [10]. The most common, serious, heart valve defect is aortic valve stenosis. This is normally an age-related disease that involves the progressive narrowing of the aortic valve. The heart has to work harder to pump enough blood to the body, eventually leading to heart muscle damage. Cardiac disability and death from congestive heart failure will result if the aortic valve cannot be reopened or replaced. Since heart valve diseases are anatomical in nature, it is challenging to address an existing valve defect from a nutritional or drug standpoint. Valve-replacement surgical procedures using prosthetic heart valves currently are the only effective long-term therapy.

Prosthetic heart valves are routinely used for replacing malfunctioning natural heart valves. The first prosthetic heart valve was introduced by Dr. Ch. Hufnagel in 1951 as a valve for replacement of malfunctioning natural heart valves [11]. More than 50 different mechanical valve designs were developed and optimized for replacement of malfunctioning natural heart valves during the last few years [12]. Today, approximately 275,000 valves worldwide and 20,000 in Germany are implanted each year [13]. About 65% of all implanted valves are mechanical valves. Even today, after five decades of prosthetic heart valves development, the main problem with these valves is the risk of thromboembolic complications. Patients with mechanical heart valves are predisposed to thromboembolic complications and must undergo lifelong anticoagulation therapy, which is related with another complication—bleeding [14, 15]. The risk of thromboembolic complications in prosthetic heart valves is mainly caused by unnatural flow with high shear stress, flow separations and flow stagnations [16]. Wherever the flow is stagnant or forms recirculation bubbles, a thrombus is likely to form, first recognized in the 19th century by German pathologist R. Virchow [3]. Another cause of thromboembolic complications is the use of foreign materials in prosthetic heart valves. Here, we consider a problem of unnatural flow conditions in the valve, which may be considered as the main cause of thromboembolic complications in prosthetic heart valves. Recently it was demonstrated that flow-induced thrombogenicity of mechanical heart valves, caused by chronic platelet activation, is an important aspect of the flow-induced blood damage. The hypothesis is that thromboembolic complications in heart valve prosthesis are initiated primarily by the nonphysiological flow conditions caused by nonanatomical valve geometry. High stresses activate and enhance the aggregation of blood platelets [17, 18]. Experiments with laser Doppler anemometry measurements revealed more than 100 times higher shear and turbulent stresses in mechanical heart valves [12]. However, the flow-induced platelet activation cannot alone explain the thrombus formation at valves. This may be explained only by a consideration of other flow phenomena—flow separations with stagnations and recirculations that are characterized by low shear and longer residence time of thromboactive substances. The design geometry of heart valve prosthesis is crucial for valve flow patterns, as shown in Figs 5, 8 and 10, and platelet activation resulted from these flow patterns [19]. That is why we first consider the designs of existing valves.

Prosthetic heart valves may be divided into different classes. Normally they are divided into two main groups of mechanical (see Fig. 5) and biological valves (see Fig. 6) and valves made of polyurethane (see Fig. 9). The two last groups mainly mimic the geometry of natural heart valves. However, from the point view of fluid mechanics it is more convenient to divide heart valves into two groups: the first group which mimics a natural valve flow consists of valves with a central flow, and the second group consists of mainly mechanical valves with one or more occluders (leaflets) located in the central flow and fixed by a hinge mechanism. All three main design concepts of mechanical valves—tilting disk valves, bileaflet valves and caged-ball valves



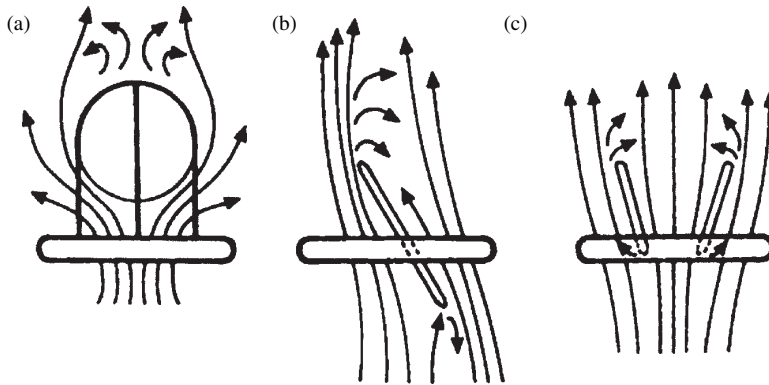


Figure 5: Schematic drawings of three main design concepts of mechanical heart valves [19]. (a) Caged-ball valve; (b) monoleaflet valve; (c) bileaflet valve.

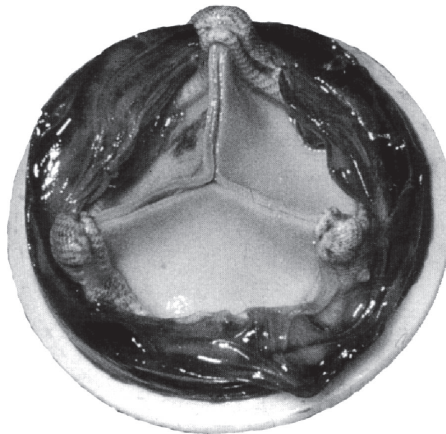


Figure 6: Photograph showing the thrombus in a biologic valve prosthesis. The thrombus is formed in the space between the leaflets and the outer wall, which are not seen in this image [21].

(see Fig. 5)—belong to the second flow concept group. However, some efforts were also directed to the development of mechanical valves with the central flow concept—applied to the bileaflet valve or, for example, a trileaflet valve called Triflo [20]. Both flow concepts have advantages and disadvantages. We will now discuss the advantages and the disadvantages of the valves of these two flow concepts.

The trileaflet biological valves, which mimic natural valve geometry with central flow concept and are made of relatively low thrombogenic material, cross-linked bovine pericardium, also generate thrombi (see Fig. 6). The number of thromboembolic complications in biological valves is nearly equal to the number in mechanical valves [15]. Figure 6 shows the thrombus that developed in the space between the leaflets and the vessel wall that is the aortic root in the case of the aortic valve. The aortic root forms some kind of diffuser (vessel enlargement) that promotes the flow separation. In this space, called the valve sinus, the blood flow is usually slow or even stagnant, which promotes the formation of thrombi. The flow separates on the leaflets' free edges forming a

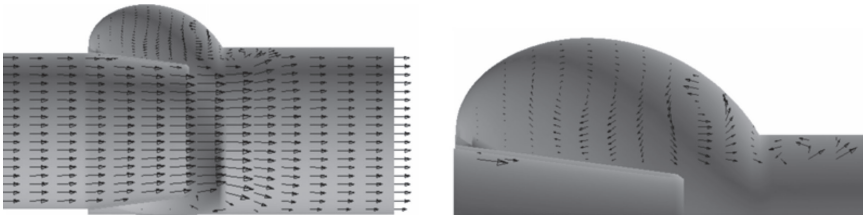


Figure 7: Vector plots of the velocity field in the central cross-section of the biological valve model. The figure on the right is an enlarged representation of the same velocity field in the sinus region.

free jet in order to be attached later to the vessel wall followed by the Coanda effect and forming a closed recirculation region or separated vortex in the sinus as shown in Fig. 7. Figure 7 shows the results of the numerical simulations in the simplified geometry of the biological trileaflet valve placed in the aortic root. The simulation was performed using the computational fluid dynamics (CFD) program FLUENT (Fluent Inc., Lebanon, NH, USA) under steady flow conditions. The Reynolds number was set to  $Re = 6000$ . The geometry was generated using the three-dimensional computer aided design (CAD) software SolidWorks (Solidworks Corp., Concord, MA, USA).

Natural valves also exhibit this flow phenomenon. But normally the endothelial cells lining the vessel wall prevent the adhesion of platelets and thrombus formation. In the case of valve replacement, an altered endothelial function and foreign materials promote thrombus formation, which may be avoided only by flow intensification. Attempts to intensify the flow in the valve sinus region can result in the change of the flow conditions—separated vortex—in the valve sinus that was earlier intended to be responsible for the valve closure. The closing mechanism of the valve was the subject of a detailed investigation and was described in a report published in 1969 as well as in later investigations [22, 23]. The flow in the valve sinus is caused by two effects: one is of viscous character and the other of inertial character. During systole, viscous forces transfer a momentum, which results in a circular flow in the sinus. Experimental investigation of the flow in the aortic valve with a dye washout method shows that the flow in the sinus is very slow. This means that viscous effects play only a minor role in the transfer of momentum from main flow to sinus flow. This having been said, a vortex is generated, but this vortex once again plays only a minor role in the closure of the leaflets. A much stronger effect is caused by inertial effects, which are generated by deceleration of the blood flow at the end of systole [24]. Hence, we can change the flow conditions in the valve sinus by changing the valve sinus geometry.

Attempts have been made to intensify the flow in the valve sinus by modifying the shape of the sinuses. Instead of three separate vortices, one uninterrupted vortex ring is created to give more space to the vortex system as shown in Fig. 8 [25]. However, this may be done only for one special case of valve application—use of valves in ventricular assist devices (VAD). In VAD one can freely design the valve housing geometry and use it as another method to intensify the flow in the sinus [24, 26]. Purge flow is generated in the sinus by redirecting the minor part of the main flow with a small protrusion formed on the valve housing. Furthermore, trileaflet valves made of polyurethane and without valve sinuses were designed (see Fig. 9). However, trileaflet valves, made of either natural material or polyurethane, have distinct advantages from a hemodynamic point of view compared with mechanical valves. These valves, if made without strong cross-section reduction, have very low pressure drop and produce low turbulence and secondary flow compared with mechanical valves.

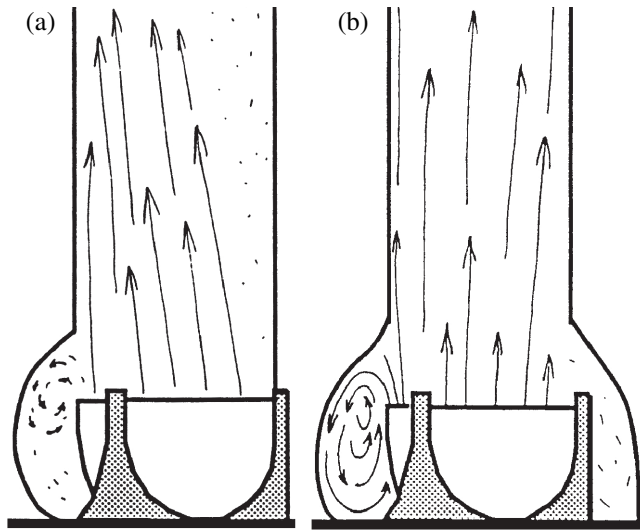


Figure 8: Intensification of the flow in sinus regions by modification of valve sinus geometry [25].  
 (a) Geometry of native biological valve with three separated vortices, one in each sinus.  
 (b) Modified geometry with space connecting all three sinuses and as such generating one large vortex ring.



Figure 9: Trileaflet heart valve prosthesis made of polyurethane. The geometry of the valve duct is designed without valve sinuses [courtesy E. Hennig, Berlin].

The three main design concepts of mechanical valves (see Fig. 5) may be divided into two groups: valves with floating and free-rotating occluders, which are limited in their motion by struts—tilting disk valve and caged-ball valve, and bileaflet valves with two occluders fixed in the space by hinge mechanisms integrated in the valve ring. Note that struts and occluders are

obstacles for blood flow. As we noted earlier all obstacles in the flow generate flow separations except flows with very low  $Re$  numbers, which is not the case for heart valves flow. The concept of the free-rotating occluders seems to be favorable because it promotes keeping the occluders free from thrombi and improves valve durability. The disadvantages of this concept are the struts or cage in the case of ball valves, which protrude in the central flow and promote thrombi formation, and the relatively higher pressure drop related with these designs. In the caged-ball valve design the high pressure drop is related to the ball resistance, whereas the high pressure drop in the tilting disk valve is related to the relatively small open angle of the occluder—about  $60^\circ$ . Such a disk position results in the formation of two strong counter-rotating vortexes and two recirculation regions beneath the occluder, where the thrombi are usually observed. Note that the region beneath the occluder may also be considered as a diffuser formed between the valve housing or vessel wall and the occluder.

In contrast, the bileaflet valve containing two occluders fixed by a hinge mechanism with an open angle of about  $85^\circ$  results in the best hemodynamic performance compared with all other mechanical valves. The most critical point related to thrombus formation and valve durability of bileaflet valves is the hinge mechanism. Some efforts were made to solve this problem, but it still a weak point of this design concept. For us the design concept with floating and free-rotating occluders seems to be more favorable and has more potential for possible flow optimization. In order to elucidate the differences in the flow behavior of the three main design concepts of mechanical valves, we generated these valve geometries using the CAD program SolidWorks and placed them in the geometric model of the aortic root (see Fig. 10). Finally, the numerical simulations of steady flow conditions with  $Re = 6000$ , plug velocity inlet profile, Newtonian blood model with kinematic viscosity of  $\nu = 3.5 \times 10^{-6} \text{ m}^2/\text{s}$  and low inlet turbulence intensity of 5% ( $k-\omega$  turbulence model was used) were performed using the CFD program FLUENT. Studies show that at shear rates higher than  $100 \text{ s}^{-1}$  blood can be considered a Newtonian fluid [21]. The most important hemodynamic parameters explaining the differences between these three valve types are collected in Table 2. Figure 10 (right) shows the distributions of the velocity magnitudes in the central cross-sections of these valves. For more convenient comparison all three valves are depicted using the same color scale. Red color indicates the areas with velocity magnitudes higher than 2 m/s that take place in monoleaflet and ball valves.

Even today there is no ideal valve with ideal hemodynamic parameters—valves with low pressure drop, low shear stress, low turbulence, and without flow separations and recirculation regions [12, 27]. One of the reasons for this is the absence of well-defined outer boundaries (vessel or ventricle wall geometry) due to strong geometry variabilities from patient to patient. Many groups have tried to develop new heart valves and optimize the heart valve flow. The main efforts for the optimization of valve flow aim to avoid or reduce flow stagnations and recirculations, or a reduction of high shear stresses.

In conclusion, the phenomenon of flow separation may play a crucial role in the alteration of the valve prosthesis function leading to the new surgical procedures for valve replacement or patient death. The flow separations in valves are caused by the same two main reasons as in engineering—obstacles in the flow, such as valve struts and occluders, and cross-section enlargement, caused by outer valve geometry that is defined by vessel or ventricle geometry. However, in contrast to the problems in engineering, the main effect of the flow separation in valves is not a higher drag and related higher pressure drop. The pressure drop in the valves is mainly defined by occluder cross-section area in the fully open position for mechanical valves and orifice area reduction for biologic valves defined by leaflets. This pressure may also significantly contribute to the required higher heart power as in the case of ball valves, and these pressure drops add a significant part to the systemic pressure. The main effect of the flow separation is a promotion of thrombus formation



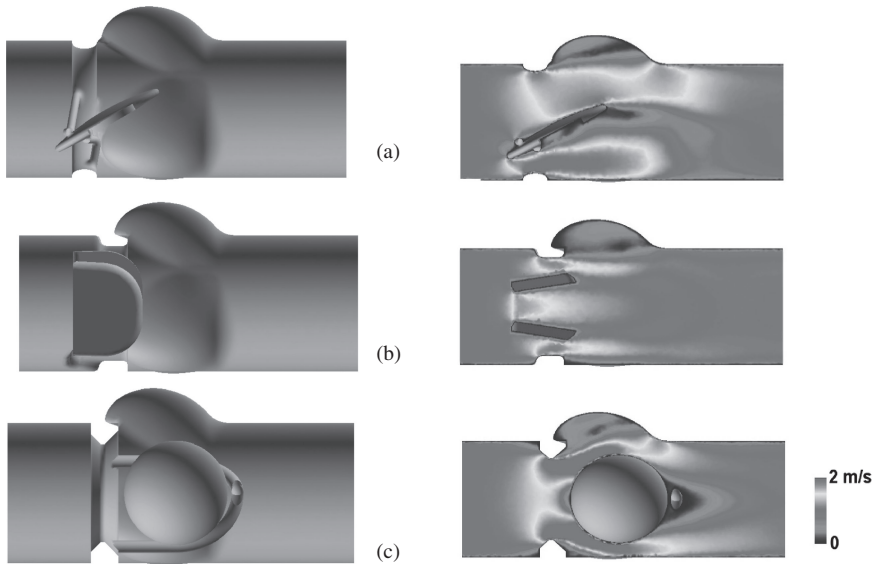


Figure 10: Left: Three-dimensional geometries of three mechanical heart valves: (a) monoleaflet valve of type Björk–Shiley Standard, (b) bileaflet valve of type St. Jude Medical and (c) caged-ball valve of type Starr–Edwards. Geometries were generated using the program SolidWorks. Right: Velocity magnitudes in the central planes of three mechanical heart valves from the results of numerical simulations: (upper) Björk–Shiley Standard valve, (middle) St. Jude Medical valve and (down) Starr–Edwards valve. Simulations were performed with CFD program FLUENT under steady flow conditions with  $Re = 6000$  and Newtonian blood fluid model. The velocity fields are represented with the same color scale. Red color indicates regions with velocity higher than 2 m/s (see Table 2).

Table 2: Some hemodynamic parameters of the three mechanical heart valves from the results of numerical simulations.

Parameters	Monoleaflet valve	Bileaflet valve	Ball valve
Pressure drop (mmHg)	9.4	5.5	22
Maximum velocity magnitude (m/s)	2.4	1.9	3
Maximum secondary velocity (m/s)	1.2	0.8	1.6
Maximum wall shear stress (Pa)	200	128	220
Maximum turbulence intensity (%)	65	47	85

in recirculation regions. This thrombus formation then causes significant higher valve narrowing with the additional danger of thromboembolic complications.

### 2.2.2 Flow separation and arteriosclerosis

As noted in Section 2.1, the vascular system is a network of vessel segments transporting blood to the organs and tissues throughout the body by convection. In other words this is our fuel pipeline.



In Section 1 we defined that a good pipeline is one with low drag or low pressure drop. In the blood circulation system the low pressure drop and hence low heart power is achieved mainly by parallel arrangement of most of the vessel segments. As noted earlier, there are two main geometric formations in the blood circulation system causing an increase in pressure drop. These are bifurcations and bends which are unavoidable in the blood vessel network system. Furthermore, there is a third formation that is caused by pathologic vessel wall alteration. This is the localized narrowing of the vessel segment, called stenosis, as a result of arteriosclerosis or thrombus formation.

Arteriosclerosis with its main organ-related diseases, e.g. ischemic heart disease, cerebrovascular disease, and others, today causes most of the deaths in countries where infectious diseases do not constitute the most important health problem [28, 29]. This disease affects the whole inner surface of the vessel system and leads to alterations of the inner walls of the blood vessels causing, later, vessel narrowing. The main risk factors, e.g. lipid disorders, hypertension, diabetes, cause functional impairment and damage to vascular cells. But the risk factors do not explain the local distribution of atherosclerotic lesions. The pattern of this distribution corresponds to zones of disturbed flow with vortex formations and low-velocity flow, which corresponds to low wall shear stress [30–34]. These flow phenomena are found in bends and bifurcations. Studies have revealed a presumably high incidence of atherosclerotic lesions in the artery bifurcations [30, 35]. Atherosclerotic lesions, which appear predisposed to form at particular sites in the complex structure of the blood circulation, mainly affect the aorta and medium-sized arteries. Among the latter, carotid bifurcations and coronary trees were the focus of attention for pathologists, because lesions are often found in these vessels, and for fluid mechanics because of their unique shape, which seems to influence the location and progress of the lesions. Furthermore, the normal functioning of carotid bifurcations is very important since their main branch *carotis interna* supplies blood to the brain. The coronary vessels are also very important because they supply blood to the heart.

Based on recent research a biological paradigm of mechanotransduction of fluid forces on the vascular wall has replaced previous mechanistic concepts. A host of knowledge has been accumulated on cell signaling pathways, which are currently thought to mediate mechanotransduction of fluid forces on blood cells and the cells lining the vascular wall. These cells are called endothelial cells and play a crucial role as mechanosensors in initiating and modulating the progress of atherosclerotic lesions. Local inflammation of the vessel wall mediates plaque growth and vascular remodeling. The wall shear stress at the vascular wall elicits a phenotype change in endothelial cells associated with humoral, metabolic, and structural changes that modulate local inflammation and adaptive remodeling. Thus wall shear stress distribution is the most important mechanical regulatory signal that links flow to adaptive changes of the vascular wall and define the distribution of locally atherosclerotic lesions [36–38].

Based on the hypothesis that information on the local shear stress pattern has prognostic value with respect to progress and risk of atherosclerotic disease, *in vivo* profiling of endothelial shear stress in coronary arteries and carotid bifurcations has been attempted recently in several studies [39–45]. Most of these studies were performed by three-dimensional reconstruction of artery segments with subsequent numerical flow simulation studies. Nowadays, CFD methods combined with realistic three-dimensional vessel reconstructions based on modern medical imaging allow the calculation of desired hemodynamic parameters under realistic boundary condition with high resolution. Numerical flow simulations are used because *in vivo* measurements of velocity profiles in the arteries are not feasible.

In order to investigate the correlation between bifurcation geometry, atherosclerotic wall alterations, and wall shear stress, the authors performed a study on human carotid bifurcations. A post mortem study, including morphometric procedure, assessment of geometric parameters and





rendered three-dimensional mathematical model of the individual vessels followed by numerical reconstruction of the blood flow were used for this investigation. Altogether 64 autopsies were performed at the Department of Pathology, General Hospital 'Dr. Carlos J. Finlay', Havana, Cuba. For each autopsy case the etiologic data about age, sex, basic disease of death and direct cause of death were collected. The age of autopsy subjects was between 22 and 92 years, and the subjects comprised both sexes 35 : 29 male/female and were free of highly infectious disease (e.g. AIDS, hepatitis). The etiologic data of all autopsy subjects were represented in detail in [46, 47]. The carotid arteries were excised carefully to obtain long distal parts of the branches, rinsed with saline and consecutively mounted in an apparatus especially designed for making vessel casts [48]. Altogether 86 vessel casts were collected from 64 autopsy subjects. After the polymer hardens, the vessel wall is cut away with a scalpel and stored for morphometric analyses. The vessel cast is an exact replica of the vessel lumen and can be used to measure geometric parameters and geometry digitalization for further numerical study using a CFD program.

Some vessel casts were digitized with the help of an optical computer-aided method for three-dimensional measurement and modeling on the basis of the structured light lines. The result of the optical digitalization is a cloud of about 20,000 points, which define the shape of the artery with 0.1 mm accuracy. These points are used to generate automatically a surface and volume of the three-dimensional artery computer model, which is used for later numerical simulation of the blood flow. Altogether, 26 vessel casts from 20 autopsy subjects were digitized for this study.

The vessel cast is employed to measure some geometric features. The diameters of all branches of carotid bifurcation were measured manually with a digital caliper (0.05 mm error). Based on the measured diameters of the carotid bifurcation, two further nondimensional geometric parameters were calculated. First, the enlargement of the internal carotid artery at its proximal part, named carotid sinus, which is responsible for the formation of the recirculation at this region [28, 49]. The enlargement parameter  $En_1$ , defined as the ratio between *carotis communis* and *carotis interna* diameters, also called the carotid sinus enlargement. A second parameter  $En_2$  defines the bifurcation enlargement. The parameter  $En_2$  is defined as the ratio of the sum of cross-sectional areas of the internal and external branches and cross-section area of the *carotis communis*, also called the total bifurcation enlargement. The projection image of a vessel cast was used to create a silhouette of the vessel geometry. This silhouette was then used to obtain information about branch angles [48]. The internal and external branch angles  $\alpha_i$  and  $\alpha_e$  were measured in two dimensions as the angle between two centerlines derived from the vessel axis in the neighborhood of the junction. The external angle was defined as the angle between *carotis communis* and *carotis externa*. The internal angle was defined as the angle between *carotis communis* and *carotis interna*. The total bifurcation angle  $\alpha$  is then defined as a sum of branch angles  $\alpha_i$  and  $\alpha_e$ . The assumption that all three branches are within the same plane leads to no more than 5% of error [50]. More detailed information about the measurements of the diameters and branch angles is presented elsewhere [48, 51]. The geometric parameters investigated in our study have been referred early to as 'geometrical risk factors' [33, 52, 53].

The vessel casts, which were digitized for reconstruction of the blood flow, were used to assess some additional geometric features. The curvature of the branches and nonplanarity of the bifurcation were assessed. The nonplanarity was defined as an angle  $\delta$  between one of the branches to the plane formed by the two other branches. In order to measure these parameters, a set of virtual cross-sections with a distance of 1 mm was generated from the digitized model of the artery. The center point of each cross section was automatically defined with help of the program NIH Image 1.55 (USA) where the mass center and the axis courses of all carotid branches were defined as a set of defined points. Each set of three neighbor points allows constructing a circle of the defined radius  $R$ . The local curvature  $C$  is then calculated as  $C = 1/R \text{ mm}^{-1}$ .



In order to reconstruct blood flow in the arteries, the digitized data of the vessel casts were imported using the software Gambit<sup>TM</sup>, which was used to create automatically an unstructured surface mesh of triangles. The surface mesh was then imported into another preprocessor TGrid (Fluent Inc.), which was used for improvement of the surface mesh and automatic generation of an unstructured computational mesh of about 400,000 tetrahedral cells. This fine mesh allows a very good resolution of the recirculation regions, i.e. an accurate calculation of wall shear stress. The computations of the stationary blood flow in reconstructed vessels with rigid walls and using a Newtonian blood fluid model were performed with the flow solver FLUENT6. The simulation is based on the three-dimensional Navier–Stokes equations for incompressible Newtonian fluid flow. All simulations were done with a second-order upwind discretization scheme for the convective terms of the Navier–Stokes equations. Pressure–velocity correction method SIMPLEC was used. The kinematic viscosity of the fluid model was set to  $3.5 \times 10^{-6} \text{ m}^2/\text{s}$ . Blood is a suspension of blood cells in plasma with a viscosity mainly defined by a hematocrit-volume fraction of red blood cells and a density of about  $1050 \text{ kg/m}^3$ . As noted in Section 2.2.1, blood can be considered as a Newtonian fluid for shear rates higher than  $100 \text{ s}^{-1}$ . The use of non-Newtonian blood models results in a decrease of the centerline velocities. However, the impact on the wall shear stress distribution may be neglected. No-slip boundary condition was set at the walls. For each artery the simulations under diastolic and systolic conditions were performed. The Reynolds number was set to  $\text{Re} = 200$  for diastole and  $\text{Re} = 700$  for systole. The inflow was defined as a parabolic velocity profile because the volume flow is normally known from measurements and because magnetic resonance imaging measurements show nearly parabolic velocity profile in the common carotid artery. The outflows were defined as constant pressures, different for each branch, thus defining the flow ratio of the internal and external carotid branches at 55:45 for systole and 75:25 for diastole [34]. The results of the numerical simulation are the flow parameters such as velocity, pressure and wall shear stress as a function of space only. If all the physiological parameters are aimed to be accounted for, i.e. pulsatile flow, compliant walls, non-Newtonian blood behavior, the CFD model becomes very complex for the study of significantly large group of vessels. Furthermore, effects of model simplifications on the assessment of the main hemodynamic parameter, the wall shear stress, were investigated in many other studies. These studies showed that steady flow simulations with rigid walls and a Newtonian blood model are accurate enough to assess the wall shear stress distribution.

In order to assess the impact of geometric parameters defining the bifurcation geometry on the risk of atherosclerotic wall alterations, we reconstructed the blood flow in 26 carotid bifurcations. In order to evaluate only geometric factors, all vessels were scaled to a constant inlet diameter, which was equal to the mean diameter of the *carotis communis*, averaged over all 86 vessel casts, of  $d = 5.6 \text{ mm}$ . The CFD studies resulted in the distributions of the wall shear stresses, being the consequence of vessel geometry as shown in Fig. 11 as a result of flow simulation under diastolic flow conditions with  $\text{Re} = 200$ . Figure 11 shows areas with very low wall shear stress, marked in blue, which corresponds to the regions of flow recirculations or flow stagnations. The color scale between 0 and 1 Pa was selected so as to underline the regions with very low wall shear stress. As a result, all areas with wall shear stress higher than 1 Pa are also marked by red color.

Finally, the comparative analysis between geometric parameters and areas with low wall shear stress was performed using the linear regression technique. The analysis showed that no correlations were found between areas with low wall shear stress and all measured angles— $\alpha_i$ ,  $\alpha_e$ ,  $\alpha$  and  $\delta$ . The square of the Pearson's correlation coefficient  $R^2$  describing the correlation from a linear regression analysis was lower than 0.001. There was no correlation found for the normalized diameter of the *carotis interna* (very low  $R^2 = 0.023$ ) distal to bifurcation. Some weak tendencies were found for the normalized diameter of the *carotis interna* or carotid sinus enlargement



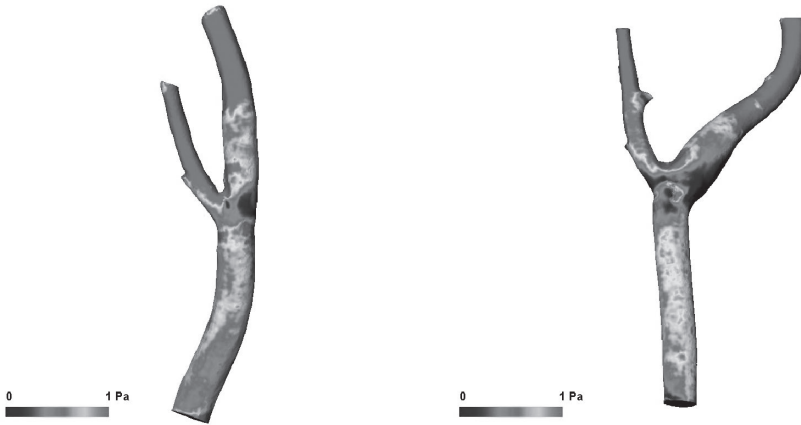


Figure 11: Distributions of wall-shear stress in two carotid bifurcations as a result of CFD simulation of flow under diastolic conditions with  $Re = 200$ . The color scale was selected so as to underline the regions with very low wall shear stress. As a result all areas with wall shear stress higher than 1 Pa are also marked in red.

En1, normalized diameter of the *carotis externa* at their proximal parts and curvatures of carotid branches. The correlation coefficients of all these parameters were about  $R^2 = 0.25$ .

A relatively high correlation coefficient with  $R^2 = 0.46$  was found only for one geometric parameter (see Fig. 12). This is the total bifurcation enlargement En2. Based on the presented correlation analysis, the total bifurcation enlargement En2 is the main risk factor among all investigated geometric parameters. First, this result seems to be surprising. However, this is a logical consequence of the fact that low wall shear stress in bifurcations is caused mainly by cross-section enlargement at that bifurcation. However, any technical duct enlargement (see Fig. 4) is characterized by the pressure loss parameter  $\zeta$  that is caused by formation of recirculation. The loss parameter is described by eqn (15) introduced in Section 2.1. If we consider the bifurcation, we can describe this as a duct enlargement depending on two geometric parameters: the total bifurcation angle being equivalent to the duct enlargement angle and the total bifurcation enlargement En2 being equivalent to the duct enlargement En. Note, that the duct enlargement the parameter  $\eta$  in eqn (15) varies between  $\eta = 0.64$  for  $\alpha = 24^\circ$  and  $\eta = 1$  for sudden expansion or  $\alpha = 180^\circ$  [9]. The investigations of the geometric parameters for 26 arteries found a mean total bifurcation angle of  $62.4$  with a standard deviation of  $\pm 17^\circ$ . Therefore, the parameter  $\eta$  varies only between 0.7 and 0.8. The mean total bifurcation enlargement En2 with standard deviation for 26 carotid bifurcations was  $1.97 \pm 0.42$ . Therefore, the parameter  $M = (En2-1)^2$  does vary significantly between 0.3 and 1.93. This is a simple fluid dynamical explanation for finding of the total bifurcation enlargement being the main geometric risk factor. In fact, the linear regression analysis performed between areas with low wall shear stress and parameter  $M$  instead of the parameter En2 revealed a higher correlation coefficient of  $R^2 = 0.55$ . Furthermore, separating the data into two groups by basic disease of death leads to an even stronger correlation in group 1 ( $R^2 = 0.83$ ) and in group 2 ( $R^2 = 0.62$ ). Group 1 includes all cases with atherosclerotic disease or hypertension disease, the disease known as a risk factor for atherogenesis, as basic disease of death. Group 2 includes all other cases.

The results obtained in our study of carotid bifurcations elucidate the effect of bifurcation with enlargement for the vascular system: This is an enlargement that generates recirculations and,



Figure 12: Linear regression analysis between surfaces ( $\text{mm}^2$ ) with low wall shear stress ( $\tau < 0.2 \text{ Pa}$ ) and the total enlargement parameter  $En2$ . The data also show large variability of carotid sinus enlargement  $En2$ , which varies between values of 1.1 and 2.8.

related to those recirculation regions, surfaces with low wall shear stress, which locally define atherosclerotic wall alterations. Analogous to the problem of thrombus formation in heart valve prosthesis for the blood circulation system and patient, which is caused by the flow separation and/or by the formation of recirculation regions (which we discussed in the Section 2.2.1), the problem for the blood circulation system, which is again caused by the formation of recirculation regions in vessels, is not a pressure drop that is caused by this phenomenon. The problem is a final vessel narrowing in the areas of atherosclerotic lesions, which finally causes a more drastic pressure drop or total blockage of the vessel.

The problem of localized development of atherosclerotic wall alterations in aorta and coronaries is of the same nature as for carotid bifurcation. The wall alterations correlate with regions of low wall shear stress. However, in aorta and coronaries the other geometric formation, bending with high curvature, plays an important role by definition of areas with recirculations and low wall shear stress. Figure 13 shows a distribution of wall shear stress in the aorta. The three-dimensional geometry of the aorta was reconstructed from the data set obtained by rotational angiography. The reconstruction was performed using the software AMIRA. The segment with high curvature in the distal part of the aorta is possibly a result of vessel alteration due to arteriosclerosis. The numerical simulation was performed with the program FLUENT under the same flow conditions as it was done for simulations in heart valve prosthesis (see Section 2.2.1). The distribution of wall shear stress shows two areas with low wall shear stress marked with blue color and located at the outer distal part and the proximal inner part downstream of the  $180^\circ$  bend. These areas of low wall shear stress were caused by aorta curvature, as shown in Fig. 5. Note that the normalized curvature of aorta is about  $R/D = 1$ , which means a relatively high loss parameter  $\zeta$ .

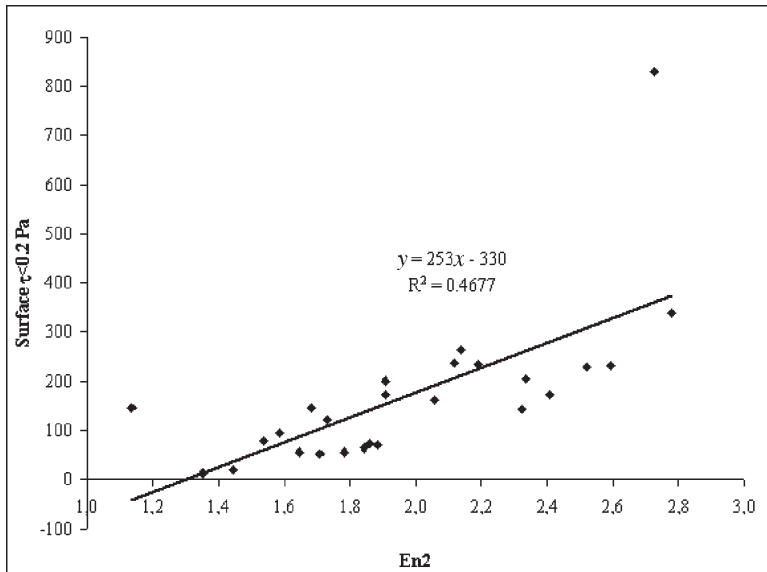


Figure 13: Distribution of the wall shear stress in the aorta as a result of CFD simulation with  $Re = 6000$ . Simulation was done with the flow solver FLUENT under steady flow conditions and the assumption of rigid walls. The unusual curvature in the aorta descendens is due to pathological deformation.

### 3 Conclusions

Flow separations are found in devices that we use in our everyday life; usually, they lower the function of the vehicle or tubing system in which they occur, but they are rarely life threatening or fatal, e.g. the flow separation at the wing of an aircraft. On the other hand, if flow separation persists in the blood flow inside the body, the cells in the vessel wall are modified and lose essential biological qualities. The vessel wall degenerates and becomes atherosclerotic. This includes a change in the vessel geometry and further aggravation of the flow separation, until blood platelets begin to circulate in the stagnation zone and deposit, ultimately blocking the vessel. In modern western society about half of the deaths are caused by the consequences of flow separation. This is a good reason for two activities: one is to investigate further these flow phenomena and the other is to keep the wall shear rate up by increasing the blood flow. This is to bring our body closer to its original design point—which is a design point of much higher physical activity, as pointed out extensively by the physiologist Heinrich [54].

### References

- [1] Tritton, D.J., *Physical Fluid Dynamics*, Oxford Science Publications, Oxford, pp. 139–152, 1995.
- [2] Leder, A., *Abgelöste Strömungen. Physikalische Grundlagen*, Vieweg Verlag, pp. 1–61, 1992.
- [3] Virchow, R., Phlogose und Thrombose im Gefaesssystem. *Gesammelte Abhandlungen zur wissenschaftlichen Medicin*, Meidinger und Sohn: Berlin, pp. 458–463, 1856.



- [4] Flachsbart, O., Geschichte der experimentellen hydro- und Aeromechanik, insbesondere der Widerstandsforschung. *Handbuch der Experimentalphysik 4*, Akademische Verlagsgesellschaft: Leipzig, pp. 1–57, 1932.
- [5] Prandtl, L., *The Mechanics of Viscous Fluids, Aerodynamic Theory*, Vol. 3, Springer-Verlag, Berlin, 1924.
- [6] Ahlborn, B.K., *Zoological Physics*, Springer-Verlag, pp. 127–158, 2004.
- [7] Caro, C.G., Pedley, T.J., Schroter, R.C. & Seed, W.A., *The Mechanics of the Circulation*, Oxford University Press: New York, Toronto, 1978.
- [8] Trautwein, W., Gauer, O.H., Koepchen, H.-P., Kreislauf des Blutes, *Herz und Kreislauf, Physiologie des Menschen*, Band 3, Urban & Schwarzenberg Verlag: München, pp. 81–264, 1972.
- [9] Sigloch, H., Technische Fluidmechanik, VDI-Verlag GmbH, pp. 94–99, 1991.
- [10] Heart Valve Disease and Therapy, <http://www.sjm.com/stjude/patients/htm/tocdis.htm>, St. Jude Medical Inc., 1997.
- [11] Hufnagel, C.A., Aortic plastic valvular prosthesis. *Bulletin of Georgetown University Medical Center*, **5**, pp. 128–130, 1951.
- [12] Yoganathan, A.P., Cardiac valve prostheses. *The Biomedical Engineering Handbook*, ed. J.D. Bronzino, CRC Press: Boca Raton, FL, pp. 1847–1870, 1995.
- [13] Frost & Sullivan, The European Heart Valve Repair Market, Report 3824, 2001.
- [14] Edmunds, L.H., Jr., Thrombotic and bleeding complications of prosthetic heart valves. *Annals of Thoracic Surgery*, **44(4)**, pp. 430–445, 1987.
- [15] Edmunds, L.H., Jr., Evolution of prosthetic heart valves. *American Heart Journals*, **141(5)**, pp. 849–55, 2001.
- [16] Bluestein, D., Research approaches for studying flow-induced thromboembolic complications in blood recirculating devices. *Expert Review of Medical Devices*, **1(1)**, pp. 65–80, 2004.
- [17] Kroll, M.H., Hellums, J.D., McIntire, L.V., Schafer, A.I. & Moake, J.L., Platelets and shear stress. *Blood*, **88(5)**, pp. 1525–1541, 1996.
- [18] Kleine, P., Perthel, M., Hasenkam, J.M., Nygaard, H., Hansen, S.B. & Laas, J., Downstream turbulence and high intensity transient signals (HITS) following aortic valve replacement with Medtronic Hall or St. Jude Medical valve substitutes. *European Journal of Cardio-Thoracic Surgery*, **17(1)**, pp. 20–24, 2000.
- [19] Yin, W., Alemu, Y., Affeld, K., Jesty, J. & Bluestein, D., Flow-induced platelet activation in bileaflet and monoleaflet mechanical heart valves. *Annals of Biomedical Engineering*, **32(8)**, pp. 1058–1066, 2004.
- [20] Sato, M., Harasaki, H., Wika, K.E., Soloviev, M.V. & Lee, A.S., Blood compatibility of a newly developed trileaflet mechanical heart valve. *ASAIO Journal*, **49(1)**, pp. 117–122, 2003.
- [21] Huang, C.R. & Fabisiak, W., A rheological equation characterizing both the time-dependent and steady state viscosity of worifice human blood. *AICHE Symposium Series*, pp. 19–21, 1978.
- [22] Bellhouse, B.J. & Talbot, L., The fluid mechanics of the aortic valve. *Journal of Fluid Mechanics*, **35**, pp. 721–735, 1969.
- [23] van Steenhoven, A.A., Veenstra, P.C. & Reneman, R.S., The effect of some hemodynamic factors on the behavior of the aortic valve. *Journal of Biomechanics*, **15**, pp. 941–950, 1982.
- [24] Affeld, K., Goubergrits, L. & Holberndt, O., Novel cardiac assist valve with a purge flow in the valve sinus. *ASAIO Journal*, **44**, pp. M642–M647, 1998.



- [25] Sturm, C., Li, W., Woodard, J.C. & Hwang, N.H., Fluid mechanics of left ventricular assist system outflow housings. *ASAIO Journal*, **38**, pp. M225–M227, 1992.
- [26] Timmel, T., Goubergrits, L. & Affeld, K., Optimization and investigation of a novel cardiac assist valve with a purge flow. *International of Journal of Artificial Organs*, **24(11)**, pp. 777–783, 2001.
- [27] Edmunds, L.H., Jr., Mckinlay, S., Anderson, J.M., Callahan, T.H., Chesebro, J.H., Geiser, E.A., Makanani, D.M., McIntire, L.V., Meeker, W.Q., Naughton, G.K., Panza, J.A., Schoen, F.J. & Didisheim, P., Directions for improvement of substitute heart valves. National Heart, Lung, and Blood Institutes Working Group report on heart valves. *Journal of Biomedical Materials Research*, **38(3)**, pp. 263–266, 1997.
- [28] Ross, R., The pathogenesis of atherosclerosis: a perspective for the 90s. *Nature*, **362**, pp. 801–809, 1993.
- [29] WHO: Atherosclerosis of the aorta and coronary arteries in 5 towns. *Bulletin of WHO*, **53**, pp. 485–645, 1976.
- [30] Asamura, T. & Karino, T., Flow patterns and spatial distribution of atherosclerotic lesions in human coronary arteries. *Circulation Research*, **66**, pp. 1045–1066, 1990.
- [31] Caro, C.G., Fitz-Gerald, J.M. & Schroter, R.C., Arterial wall shear and distribution of early atheroma in man. *Nature*, **223**, p. 1159, 1969.
- [32] Friedman, M.H., Hutchins, G.M., Bargeron, C.B., Deters, O.J. & Mark, F.F., Correlation between intimal thickness and fluid shear in human arteries. *Atherosclerosis*, **39**, pp. 425–436, 1981.
- [33] Friedman, M.H., Variability of 3D arterial geometry and dynamics, and its pathologic implications. *Biorheology*, **39(3, 4)**, pp. 513–517, 2002.
- [34] Ku, D.K., Giddens, D.P., Zarins, C.K. & Glagov, S., Pulsatile flow and atherosclerosis in the human carotid bifurcation. Positive correlation between plaque location and low and oscillating shear stress. *Arteriosclerosis*, **5(3)**, pp. 293–302, 1985.
- [35] Frangos, S.G., Localization of atherosclerosis. *Archives of Surgery*, **134**, pp. 1142–1149, 1999.
- [36] Dai, G., Kaazempur-Mofrad, M.R., Natarajan, S., Zhang, Y., Vaughn, S., Blackman, B.R., Kamm, R.D., Garcia-Cardena, G. & Gimbrone, M.A., Jr., Distinct endothelial phenotypes evoked by arterial waveforms derived from atherosclerosis-susceptible and -resistant regions of human vasculature. *Proceedings of the National Academy of Sciences, USA*, **101**, pp. 14871–14876, 2004.
- [37] Ohura, N., Yamamoto, K., Ichioka, S., Sokabe, T., Nakatsuka, H., Baba, A., Shibata, M., Nakatsuka, T., Harii, K., Wada, Y., Kohro, T., Kodama, T. & Ando, J., Global analysis of shear stress-responsive genes in vascular endothelial cells. *Journal of Atherosclerosis and Thrombosis*, **10**, pp. 304–313, 2003.
- [38] Tedgui, A., Lehoux, S. & Levy, B., Mechanical factors and vascular biology. *Biology of the Arterial Wall*, eds. B.I. Levy & A. Tedgui, Kluwer Academic Publishers: Dordrecht, 1st edn, pp. 71–100, 1999.
- [39] Bom, N., de Korte, C.L., Wentzel, J.J., Krams, R., Carlier, S.G., van der Steen, A.W., Slager, C.J. & Roelandt, J.R., Quantification of plaque volume, shear stress on the endothelium, and mechanical properties of the arterial wall with intravascular ultrasound imaging. *Z. Kardiol.*, **89(2)**, pp. 105–111, 2000.
- [40] Feldman, C.L., Ilegbusi, O.J., Hu, Z., Nesto, R., Waxman, S. & Stone, P.H., Determination of *in vivo* velocity and endothelial shear stress patterns with phasic flow in human coronary arteries: a methodology to predict progression of coronary atherosclerosis. *American Heart Journal*, **143**, pp. 931–939, 2002.



- [41] Goubergrits, L., Affeld, K., Wellnhofer, E., Zurbrugg, R. & Holmer, T., Estimation of wall shear stress in bypass grafts with computational fluid dynamics method. *International Journal of Artificial Organs*, **24**, pp. 145–151, 2001.
- [42] Hoffmann, K.R., Wahle, A., Pellot-Barakat, C., Sklansky, J. & Sonka, M., Biplane X-ray angiograms, intravascular ultrasound, and 3D visualization of coronary vessels. *International Journal of Cardiac Imaging*, **15**, pp. 495–512, 1999.
- [43] Ilegbusi, O.J., Hu, Z., Nesto, R., Waxman, S., Cyganski, D., Kilian, J., Stone, P.H. & Feldman, C.L., Determination of blood flow and endothelial shear stress in human coronary artery *in vivo*. *Journal of Invasive Cardiology*, **11**, pp. 667–674, 1999.
- [44] Krams, R., Wentzel, J.J., Oomen, J.A., Vinke, R., Schuurbiens, J.C., de Feyter, P.J., Serruys, P.W. & Slager, C.J., Evaluation of endothelial shear stress and 3D geometry as factors determining the development of atherosclerosis and remodeling in human coronary arteries *in vivo*. Combining 3D reconstruction from angiography and IVUS with computational fluid dynamics. *Arterioscler, Thrombosis and Vascular Biology*, **17**, pp. 2061–2065, 1997.
- [45] Stone, P.H., Coskun, A.U., Yeghiazarians, Y., Kinlay, S., Popma, J.J., Kuntz, R.E. & Feldman, C.L., Prediction of sites of coronary atherosclerosis progression: *in vivo* profiling of endothelial shear stress, lumen, and outer vessel wall characteristics to predict vascular behaviour. *Current Opinion in Cardiology*, **18**, pp. 458–470, 2003.
- [46] Goubergrits, L., Affeld, K., Fernandez-Britto, J. & Falkon, L., Atherosclerosis in the human common carotid artery. A morphometric study of 31 specimens. *Pathology Research and Practice*, **197**, pp. 803–809, 2001b.
- [47] Goubergrits, L., Affeld, K., Fernandez-Britto, J. & Falkon L., Geometry of the human common carotid artery. A vessel cast study of 86 specimens. *Pathology Research and Practice*, **198**, pp. 543–551, 2002.
- [48] Affeld, K., Goubergrits, L., Fernandez-Britto, J. & Falkon, L., Variability of the geometry of the human common carotid artery. A vessel cast study of 31 specimens. *Pathology Research and Practice*, **194**, pp. 597–602, 1998b.
- [49] Balasubramanian, K., An experimental investigation of steady flow at an arterial bifurcation, Ph.D. thesis, Georgia Institute of Technology, Atlanta, 1979.
- [50] Forster, F.K., Chikos, P.M. & Frazier, J.S., Geometric modeling of the carotid bifurcation in humans. Implications in ultrasonic Doppler and radiologic investigations. *Journal of Clinical Ultrasound*, **13**, pp. 385–390, 1985.
- [51] Goubergrits, L., Affeld, K., Fernandez-Britto, J. & Falkon, L., Investigation of geometry and atherosclerosis in the human carotid bifurcation's. *Journal of Mechanical in Medicine and Biology*, **3(1)**, pp. 31–48, 2003.
- [52] Perktold, K. & Resch, M., Numerical flow studies in human carotid artery bifurcations: basic discussion of the geometric factor in atherogenesis. *Journal of Biomedical Engineering*, **12**, pp. 111–123, 1989.
- [53] Friedman, M.H., Deters, O.J., Mark, F.F., Barger, C.B. & Hutchins, G.M., Arterial geometry affects hemodynamics. A potential risk factor for atherosclerosis. *Atherosclerosis*, **46**, pp. 225–231, 1983.
- [54] Heinrich, B., *Why We Run*, HarperCollins Publishers: New York, 2002.

